



## Smooth and robust multi-mode shaped commands

Abdullah Alshaya <sup>\*</sup>, Khaled Alhazza

Mechanical Engineering Department, College of Engineering and Petroleum, Kuwait University, PO Box 5969, Safat 13060, Kuwait

### ARTICLE INFO

Communicated by X. Jing

**Keywords:**

Command-shaping  
Vibration control  
Multi-mode system  
Open-loop control  
Residual vibration  
Sloshing suppression

### ARTICLE INFO

Smooth robust shaped commands with general polynomial and waveform profiles are proposed for eliminating residual vibrations in multi-mode damped systems. The command time length of the proposed commands is selectable which helps in designing an optimum command that results of a desired reduction in the induced transient vibration, utilizes the maximum input capability of the actuator, and enhances the command robustness to the uncertainties in the system parameters. The commands are generated using the system natural frequencies and damping ratios. This is attractive for complicated multi-mode damped systems where mathematical models are difficult to derive. The continuous-time profiles of the proposed commands that are based on the monomial and Fourier bases render the possibility of enhancing the robustness and smoothness in order to eliminate jerks, i.e., inrush current, and inaccurate timing and delay of the actuator. The efficacy of their performance in eliminating residual vibrations is validated using numerical simulations and experiment. Their sensitivity to system modeling uncertainties is further reduced using three different approaches; relaxing the command length, flattening the sensitivity curve at and adjacent to the modeling frequencies, and introducing virtual frequencies adjacent to the design frequencies to enhance the bandwidth of the reduced sensitivity region.

### 1. Introduction

Controlling techniques are extensively used in modern industrial automated systems that consist of rest-to-rest maneuvers such as in robotic manipulation, automotive and space industries. These maneuvers are usually used in automated lines and repeated cycles. Implementation of such techniques helps in controlling the induced transient and residual vibrations, enhances the accuracy of the maneuver, and ultimately leads to faster, safer, and cost effective operations. Vibration and oscillation control of flexible dynamic systems becomes a challenging control problem when considering multi-mode systems. Unlike feedback control that necessitates the need of acquiring real-time measurements of the vibrational modes, open-loop techniques are alternatively used for free residual vibration maneuver. Targeting the primary mode and assuming low energy levels in higher modes does not guarantee a complete elimination of residual vibrations. Therefore, shaped commands for controlling the induced vibrations in multi-mode systems becomes necessary especially with the introduction of new generation of powerful and fast actuators.

Command shaping technique, which is an open-loop technique, is based on designing a carefully shaped system command that results of free residual vibration in a rest-to-rest maneuver. These trajectories are usually designed by either convolving what is known as input shapers with a general input command or producing such shaped command that satisfies the system constrains using optimization techniques [1–6]. The major disadvantages of the command designed using the input shapers are the generated steps in their command profile, the sensitivity to modeling errors, and the dependence of the command time length on the system

\* Corresponding author.

E-mail addresses: [abdullah.alshaye@ku.edu.kw](mailto:abdullah.alshaye@ku.edu.kw) (A. Alshaya), [kalhazza@vt.edu](mailto:kalhazza@vt.edu) (K. Alhazza).

parameters. Even though a smooth reference command can be used, the convolution of the input shapers increases the command rise time [7,8]. Robust input shapers necessitate the need of using multiple impulses which leads to several unwanted jerks in the command and increase in the rise time [9,10].

The input shaping controls were extended to a multi-mode system using what are known as convolved shapers and simultaneous shapers [1,11,12]. Convolved input shaper is based on generating a shaped input command by convolving its reference input with multiple sequences of impulses that are designed for each of the vibrational modes. For system with many vibrational modes and high frequencies, the convolved shaper will consist of packed impulses that are difficult to implement in real time due to bandwidth limitation. Alternatively, simultaneous input shaper is designed from a set of simultaneous non-linear constraint equations to generate a sequence with less impulses than the convolved shaper has and, hence, much faster. However, the time locations of these generated impulses in these two shapers may not be within the sampling time of the actuator hardware which degrades the shaper performance. Furthermore, the resultant multiple steps in the convolved shaper can be reduced by using a smooth original command. The latter was demonstrated to eliminate residual vibrations of multi-mode systems [13–15]. However, the most drawbacks of these multi-mode input shapers are their designing difficulties, limitation of utilizing the full capabilities of the actuator, and the reduction of the servo rate performance due to multiple jerks that results from multiple impulses.

Single-mode input shapers could also be combined with different types of filters such as multi-notch, low-pass, band-stop, and time-delay filters to tune frequencies of a multi-mode system [16–19]. However, a common frequency has to be found such that all the modes of the multi-mode system are odd-multiples of that frequency [20]. Such other techniques, e.g. input–output inversion technique, model reference command shaping, time-optimal anti-swing control, necessitate the need of knowing the exact system model to control multi-mode flexible systems [21–25]. Even though the input command that is designed based on the time-optimal control has smaller maneuver duration (faster response), it produces large transient oscillations and has higher sensitivity to modeling errors [26]. Furthermore, adaptive tracking control method subjected to parametric uncertainties and external disturbances was utilized to control two-degree-of-freedom system [27,28].

Step commands tend to include multiple impulses and large number of jerks in their shaped profiles that could affect the actuator in a long-term [12]. Impulses degrade the motor performance due to actuation delay and mismatch timing while jerks short the actuator life expectancy due to large inrush current and increase maintenance. Discretization of shaped commands into smaller time steps based on the sampling actuator rate could degrade the command performance and result of inaccurate positioning. Recently, shaped commands in form of multiple steps profile [29,30], cosine and sine waves [31,32], and polynomial profile [33] were introduced to mitigate the residual vibrations in multi-mode systems. The need of extending such commands and introducing new continuous-time functions that are based on the general monomial and Fourier bases while considering the damping effects with adjustable-smoothness and robustness conditions becomes necessary.

The main contribution of this work is to propose *smooth* and *robust* shaped multi-mode commands that eliminate residual vibrations in all the vibrational modes with the presence of damping. In real life applications, smooth commands based on a continuous-time profile can be easily discretized using modern digital control systems. Two different general profiles based on polynomial and waveform functions are developed and compared. Without the full knowledge of the system model, only the system natural frequencies and damping ratios are needed to generate these shaped commands. The command time length can be selected based on the required reduction in the transient vibration amplitudes, the command robustness to the system uncertainties, and the hardware sampling rates to help avoiding the command mismatch issue. This makes the command shaping more attractive than the classical input shapers. The effectiveness and performance of these shaped commands are tested to suppress sloshing in a moving water-filled container and to eliminate residual oscillations in a multiple pendulum system. The robustness are enhanced by adding zero derivative constraint of the sensitivity curve at the modeling frequencies to flatten the insensitivity spectrum, introducing virtual frequencies adjacent to the design frequencies to enhance the robustness range, and relaxing the command time length.

## 2. Command designing

A multi-mode damped linear system of order  $N$  that is subjected to a single input can be written in terms of its principal (uncoupled) modal coordinates,  $q_i(t)$ , as

$$\ddot{q}_i(t) + 2\zeta_i \omega_{n,i} \dot{q}_i(t) + \omega_{n,i}^2 q_i(t) = p_i f(t), \quad \text{for } i = 1, 2, \dots, N \quad (1)$$

where  $\omega_{n,i}$  and  $\zeta_i$  are the principal natural frequencies and damping ratios of the multi-mode system,  $p_i$  is a forcing vector, and  $f(t)$  is the system single input. The following subsections demonstrate the general multi-mode system response when using different general system inputs. Once the system response is known, the system input profile can be designed such that it eliminates the system residual vibrations from all the excited vibrational modes at the end of the command duration. It is worth mentioning that the multi-mode systems are generally nonlinear but they can be approximated by linear systems. This type of mathematical analyses can be applied on many systems such cranes, moving liquid-filled container, and translating and rotating beams.

### 2.1. Polynomial input command (PIC)

A general  $m$ -order polynomial profile is firstly considered,

$$f(t) = \sum_{k=0}^m a_k t^k \quad (2)$$

where  $a_k$  is the polynomial coefficients. Upon substitution of Eq. (2) into Eq. (1), the complete general solutions of  $q_i(t)$  and its time derivatives, assuming zero initial conditions, are

$$q_i(t) = \left[ 1 + \frac{\sigma_{1,i}e^{\sigma_{2,i}t} - \sigma_{2,i}e^{\sigma_{1,i}t}}{\sigma_{2,i} - \sigma_{1,i}} \right] b_{i,0} + \left[ t - \frac{e^{\sigma_{2,i}t} - e^{\sigma_{1,i}t}}{\sigma_{2,i} - \sigma_{1,i}} \right] b_{i,1} + \sum_{k=2}^m b_{i,k} t^k \quad (3a)$$

$$\dot{q}_i(t) = \left[ \frac{\sigma_{1,i}\sigma_{2,i}(e^{\sigma_{2,i}t} - e^{\sigma_{1,i}t})}{\sigma_{2,i} - \sigma_{1,i}} \right] b_{i,0} + \left[ 1 - \frac{\sigma_{2,i}e^{\sigma_{2,i}t} - \sigma_{1,i}e^{\sigma_{1,i}t}}{\sigma_{2,i} - \sigma_{1,i}} \right] b_{i,1} + \sum_{k=2}^m k b_{i,k} t^{k-1} \quad (3b)$$

where  $\sigma_{1,i}, \sigma_{2,i} = -\zeta_i \omega_{n,i} \pm \omega_{n,i} \sqrt{\zeta_i^2 - 1}$  and  $b_{i,k} = \mathbf{b}_i = \{b_{i,0} \ b_{i,1} \ \dots \ b_{i,m}\}^T$  is a  $(m+1)$ -column vector for ever mode  $i$ . The latter,  $b_{i,k}$ , is related to the coefficients of the PIC,  $a_k$ , in a recursive relation that can expressed in a matrix form as

$$\mathbf{b}_i = p_i \mathbf{T}_i^{-1} \mathbf{a}, \quad \text{where} \quad \mathbf{T}_i(k, j) = \begin{cases} \omega_{n,i}^2, & j = k \\ 2k\zeta_i \omega_{n,i}, & j = k+1 \\ k(k+1), & j = k+2 \\ 0, & \text{otherwise} \end{cases} \quad (4)$$

where  $\mathbf{T}_i$  is a  $(m+1)$ -square matrix and  $\mathbf{a} = \{a_0 \ a_1 \ \dots \ a_m\}^T$  is  $(m+1)$ -column vector corresponding to the coefficients of the PIC. Since the objective of the PIC is to eliminate the residual vibrations from all the excited vibrational modes at the end of the command duration, setting  $q_i(\tau) = 0$  and  $\dot{q}_i(\tau) = 0$  gives two sets of  $N$  conditions that can be written as,

$$\begin{Bmatrix} q_1(\tau) \\ \dot{q}_1(\tau) \\ \vdots \\ q_N(\tau) \\ \dot{q}_N(\tau) \end{Bmatrix} = \begin{Bmatrix} \mathbf{L}_i^T \mathbf{b}_1 \\ \dot{\mathbf{L}}_i^T \mathbf{b}_1 \\ \vdots \\ \mathbf{L}_N^T \mathbf{b}_N \\ \dot{\mathbf{L}}_N^T \mathbf{b}_N \end{Bmatrix} = \begin{Bmatrix} p_1 \mathbf{L}_1^T \mathbf{T}_1^{-1} \\ p_1 \dot{\mathbf{L}}_1^T \mathbf{T}_1^{-1} \\ \vdots \\ p_N \mathbf{L}_N^T \mathbf{T}_N^{-1} \\ p_N \dot{\mathbf{L}}_N^T \mathbf{T}_N^{-1} \end{Bmatrix} \mathbf{a} = \mathcal{P} \mathbf{a} = \mathbf{0} \quad (5)$$

where  $\mathcal{P}$  is rectangular matrix of size  $2N \times (m+1)$  and the two  $(m+1)$  column vectors  $\mathbf{L}_i$  and  $\dot{\mathbf{L}}_i$  are the corresponding right terms of Eqs. (3) at  $t = \tau$ , namely

$$\begin{aligned} \mathbf{L}_i(1) &= 1 + \frac{\sigma_{1,i}e^{\sigma_{2,i}\tau} - \sigma_{2,i}e^{\sigma_{1,i}\tau}}{\sigma_{2,i} - \sigma_{1,i}} \\ \mathbf{L}_i(2) &= \tau - \frac{e^{\sigma_{2,i}\tau} - e^{\sigma_{1,i}\tau}}{\sigma_{2,i} - \sigma_{1,i}} \end{aligned} \quad (6)$$

$$\mathbf{L}_i(k+1) = \tau^k, \quad \text{for } k = 2, 3, \dots, m$$

and

$$\begin{aligned} \dot{\mathbf{L}}_i(1) &= \frac{\sigma_{1,i}\sigma_{2,i}(e^{\sigma_{2,i}\tau} - e^{\sigma_{1,i}\tau})}{\sigma_{2,i} - \sigma_{1,i}} \\ \dot{\mathbf{L}}_i(2) &= 1 - \frac{\sigma_{2,i}e^{\sigma_{2,i}\tau} - \sigma_{1,i}e^{\sigma_{1,i}\tau}}{\sigma_{2,i} - \sigma_{1,i}} \\ \dot{\mathbf{L}}_i(k+1) &= k\tau^{k-1}, \end{aligned} \quad (7)$$

To avoid the sudden change on the system input at the beginning and the end of the command duration, the input has to start from zero and end at zero, i.e.,  $f(0) = 0$  and  $f(\tau) = 0$ . Furthermore, the time derivatives of the input command could also be set equal to zero at the beginning and the end of command interval to further smooth the input and the response, i.e.,  $\dot{f}(0) = 0$  and  $\dot{f}(\tau) = 0$ . Additional physical constraints on the system input in terms of its maximum velocity, power, and/or force, have also to be imposed. The interpretation of the system and the input command defines the control target which is generally imposed mathematically in term of the total integral of the shaped command, namely

$$\int_0^\tau f(t) dt = \sum_{k=0}^m \frac{a_k}{k+1} \tau^{k+1} = U \quad (8)$$

where  $U$  is the input capability reached at the end of the command,  $t = \tau$ . It is worth mentioning that the form of constraint is not only limited in term of the total integral where other forms can also be used.

Imposing the  $2N$  constraints of zero residual vibrations, Eq. (5), and the five system input constraints (the four smoothness conditions and the total integral constraint) results of the following linear system of simultaneous equations,

$$\begin{Bmatrix} \mathcal{P} \\ 1 & 0 & 0 & \dots & 0 & 0 & 0 \\ 1 & \tau & \tau^2 & \dots & \tau^{m-2} & \tau^{m-1} & \tau^m \\ 0 & 1 & 0 & \dots & 0 & 0 & 0 \\ 0 & 1 & 2\tau & \dots & (m-2)\tau^{m-3} & (m-1)\tau^{m-2} & m\tau^{m-1} \\ \tau & \frac{\tau^2}{2} & \frac{\tau^3}{3} & \dots & \frac{\tau^{m-1}}{m-1} & \frac{\tau^m}{m} & \frac{\tau^{m+1}}{m+1} \end{Bmatrix} \begin{Bmatrix} a_0 \\ a_1 \\ \vdots \\ a_{m-1} \\ a_m \end{Bmatrix} = \begin{Bmatrix} \mathbf{0}_{2N \times 1} \\ 0 \\ 0 \\ 0 \\ 0 \\ U \end{Bmatrix} \quad (9)$$

Therefore, a polynomial of order  $m = 2N + 4$  are needed in Eq. (2) to satisfy these essential constraints, Eq. (9). Since the matrix  $\mathcal{P}$  is only function of the natural frequencies and damping ratios, the coefficients of the PIC,  $\mathbf{a} = \mathbf{a}_k$ , are determined using only these parameters without the full knowledge the mathematical model of the multi-mode damped system. This is really attractive for controlling complex systems where their mathematical models are hard to derive, and therefore, their corresponding natural frequencies and damping ratios can be alternatively determined using experimental modal analysis [34]. The command time length,  $\tau$ , is independent from the system parameters and can be selected to give an optimum input profile, i.e., faster maneuver than the classical input shapers. Even though decreasing the command length will consequently make the response faster, it will increase the system sensitivity to the system parameters uncertainties, and hence, affect the overall performance. In general, the command length is selected based on the system input capability, e.g., sampling time of actuator hardware and/or its maximum capability, and the total traveled distance.

## 2.2. Waveform input command (WIC)

The general form of a waveform input command expressed as a Fourier series expansion is considered,

$$f(t) = \frac{a_0}{2} + \sum_{k=1}^m a_k \cos\left(\frac{2\pi kt}{\tau}\right) + \sum_{k=1}^m b_k \sin\left(\frac{2\pi kt}{\tau}\right) \quad (10)$$

where  $\tau$  here is the command duration, and  $a_0$ ,  $a_k$ , and  $b_k$  are the unknown Fourier coefficients. Assuming zero initial conditions, the complete general responses of the waveform input command of a multi-mode underdamped system are

$$\begin{aligned} q_i(t) &= \frac{p_i}{\omega_{n,i}^2} \left[ \frac{a_0}{2} + \sum_{k=1}^m \frac{a_k}{\sqrt{(1-k^2r^2)^2 + (2k\zeta_i r)^2}} \cos\left[\frac{2\pi k}{\tau}t - \tan^{-1}\left(\frac{2k\zeta_i r}{1-k^2r^2}\right)\right] \right. \\ &\quad \left. + \sum_{k=1}^m \frac{b_k}{\sqrt{(1-k^2r^2)^2 + (2k\zeta_i r)^2}} \sin\left[\frac{2\pi k}{\tau}t - \tan^{-1}\left(\frac{2k\zeta_i r}{1-k^2r^2}\right)\right] \right] \end{aligned} \quad (11a)$$

$$\begin{aligned} \dot{q}_i(t) &= \frac{p_i}{\omega_{n,i}^2} \left[ \sum_{k=1}^m \frac{-2\pi k a_k}{\tau \sqrt{(1-k^2r^2)^2 + (2k\zeta_i r)^2}} \sin\left[\frac{2\pi k}{\tau}t - \tan^{-1}\left(\frac{2k\zeta_i r}{1-k^2r^2}\right)\right] \right. \\ &\quad \left. + \sum_{k=1}^m \frac{2\pi k b_k}{\tau \sqrt{(1-k^2r^2)^2 + (2k\zeta_i r)^2}} \cos\left[\frac{2\pi k}{\tau}t - \tan^{-1}\left(\frac{2k\zeta_i r}{1-k^2r^2}\right)\right] \right] \end{aligned} \quad (11b)$$

where  $r = 2\pi/(\tau\omega_{n,i})$ . Similar to PIC, setting  $t = \tau$  in Eq. (11) guarantees the elimination of the residual vibration from all the vibrational modes. These conditions can written as

$$\begin{bmatrix} q_1(\tau) \\ \dot{q}_1(\tau) \\ \vdots \\ q_N(\tau) \\ \dot{q}_N(\tau) \end{bmatrix} = \mathcal{W} \begin{bmatrix} a_0 \\ a_1 \\ b_1 \\ \vdots \\ a_m \\ b_m \end{bmatrix} = \mathcal{W}\mathbf{c} = \mathbf{0} \quad (12)$$

where vector  $\mathbf{c}$  contains the Fourier coefficients,  $a_0$ ,  $a_k$ , and  $b_k$ , and the entries of the  $2N \times (2m+1)$ -rectangular matrix  $\mathcal{W}$  are defined as

$$\begin{aligned} \mathcal{W}(2i-1, 1) &= \frac{p_i}{2\omega_{n,i}^2} \\ \mathcal{W}(2i-1, 2k) &= \frac{p_i}{\omega_{n,i}^2 \sqrt{(1-k^2r^2)^2 + (2k\zeta_i r)^2}} \cos\left[\frac{2\pi k}{\tau}t - \tan^{-1}\left(\frac{2k\zeta_i r}{1-k^2r^2}\right)\right] \\ \mathcal{W}(2i-1, 2k+1) &= \frac{p_i}{\omega_{n,i}^2 \sqrt{(1-k^2r^2)^2 + (2k\zeta_i r)^2}} \sin\left[\frac{2\pi k}{\tau}t - \tan^{-1}\left(\frac{2k\zeta_i r}{1-k^2r^2}\right)\right] \\ \mathcal{W}(2i, 1) &= 0 \\ \mathcal{W}(2i, 2k) &= -\frac{2\pi p_i k}{\tau \omega_{n,i}^2 \sqrt{(1-k^2r^2)^2 + (2k\zeta_i r)^2}} \sin\left[\frac{2\pi k}{\tau}t - \tan^{-1}\left(\frac{2k\zeta_i r}{1-k^2r^2}\right)\right] \\ \mathcal{W}(2i, 2k+1) &= \frac{2\pi p_i k}{\tau \omega_{n,i}^2 \sqrt{(1-k^2r^2)^2 + (2k\zeta_i r)^2}} \cos\left[\frac{2\pi k}{\tau}t - \tan^{-1}\left(\frac{2k\zeta_i r}{1-k^2r^2}\right)\right] \end{aligned} \quad (13)$$

where  $i = 1, 2, \dots, N$  and  $k = 1, 2, \dots, m$ . Enforcing smoothness conditions,

$$f(0) = f(\tau) = \frac{a_0}{2} + \sum_{k=1}^m a_k = 0 \quad (14a)$$

$$\dot{f}(0) = \dot{f}(\tau) = \sum_{k=1}^m k b_k = 0 \quad (14b)$$

Finally, the total integral constraint of the command over its duration gives

$$\int_0^\tau f(t) dt = \frac{\tau a_0}{2} = U \quad (15)$$

and from which the value of  $a_0$  can be determined. Therefore, the other  $2N + 2$  conditions from the zero residual vibration and smoothness conditions necessitate the need of retaining  $m = N + 1$  terms in the Fourier series. Adding all the system and input constraints, one can construct the following linear system of simultaneous equations to determine the values of  $a_0$ ,  $a_k$ , and  $b_k$ , namely

$$\begin{bmatrix} & \mathbf{W} \\ \frac{1}{2} & 1 & 0 & 1 & 0 & \cdots & 1 & 0 \\ 0 & 0 & 1 & 0 & 2 & \cdots & 0 & m \\ \tau/2 & 0 & 0 & 0 & 0 & \cdots & 0 & 0 \end{bmatrix} \begin{Bmatrix} a_0 \\ a_1 \\ b_1 \\ a_2 \\ b_2 \\ \vdots \\ a_m \\ b_m \end{Bmatrix} = \begin{Bmatrix} \mathbf{0}_{2N \times 1} \\ 0 \\ 0 \\ U \end{Bmatrix} \quad (16)$$

It is worth noting that one also could use one form of either sine or cosine waves to reduce the number of constraint equations, and hence, the number of retained terms [31,32]. However, this of course will restrict the freedom of extending the smoothness of the input profile and restrict the enhancing of the command robustness as will be demonstrated in the following section.

### 3. Robustness

The system frequencies and damping ratios are either determined from a derived model or measured experimentally. Usually, derived models give approximate values of the natural frequencies due to the applied assumptions upon derivation. Similarly, experimental determined values could also involve some errors due to the approximate estimation of the system parameters and the limitation in the test measurements. Furthermore, variations in one or more of the natural frequencies during maneuver will result of increase in the residual vibrations. Therefore, it is necessary to assess how these changes in the natural frequencies and damping ratios affect the performance of the shaped commands and enhance their robustness to the system errors and uncertainties.

The ability of the shaped commands to reduce residual vibrations in the presence of modeling errors is usually used as a measure of the command robustness or insensitivity. The command robustness under variations of the system natural frequencies and damping ratios can be enhanced using several ways (including but not limited to); increasing the command time length, adding additional constraints based on minimizing residual amplitudes at or near the modeled frequencies, and/or widening the robustness range by introducing additional virtual frequencies adjacent to the operating frequency. Mathematically, the residual vibration amplitude at the end of the command duration in terms of the principal coordinates is defined as follows,

$$\text{Vib. Amp.} = \sum_{i=1}^N \sqrt{q_i^2(\tau) + \left( \frac{\dot{q}_i(\tau)}{\omega_{n,i}} \right)^2} \quad (17)$$

Imposing additional constraints based on setting the derivatives of the residual vibration amplitude with respect to the system frequencies,  $\omega_{n,i}$ , to zero, i.e.,  $d(\text{Amp})/d\omega_{n,i} = 0$ , reduces the induced residual vibrations at the vicinity of that frequency. For PIC, this condition is satisfied if

$$\frac{\partial q_i(\tau)}{\partial \omega_{n,i}} = \left( \frac{\partial \mathbf{L}_i^T}{\partial \omega_{n,i}} \mathbf{T}_i^{-1} + \mathbf{L}_i^T \frac{\partial \mathbf{T}_i^{-1}}{\partial \omega_{n,i}} \right) \mathbf{a} = 0, \quad \forall i \quad (18a)$$

$$\frac{\partial (\dot{q}_i(\tau)/\omega_{n,i})}{\partial \omega_{n,i}} = \left( \frac{\partial (\dot{\mathbf{L}}_i^T / \omega_{n,i})}{\partial \omega_{n,i}} \mathbf{T}_i^{-1} + \dot{\mathbf{L}}_i^T \frac{\partial (\mathbf{T}_i^{-1} / \omega_{n,i})}{\partial \omega_{n,i}} \right) \mathbf{a} = 0, \quad \forall i \quad (18b)$$

Therefore,  $2N$  conditions have to be additional imposed to enhance the robustness at the vicinity of all the natural frequencies. The same concepts can be applied to WIC. To avoid retaining higher order polynomial and increase in the command time length, the zero derivative constraints could only be imposed at certain frequencies. The concepts of designing shaped commands based on rest-to-rest conditions and zero residual vibration and zero derivative of the sensitivity curve are similar, respectively, to the concepts of zero-vibration (ZV) and zero-vibration and derivative (ZVD) input shapers.

Another approach of improving command robustness is to use higher order shaped command profiles with lower order system in order to increase the bandwidth of the insensitivity range. This can be achieved by introducing two virtual frequencies distributed around the system design frequencies while either removing or maintaining the original frequencies in the shaped command profiles. Therefore, these approaches will double and triple the order of the shaped commands, respectively. Unlike the classical command shaping techniques where increasing shaped command order will increase the computations needed to generate such profiles, the proposed commands can be easily designed from solving a system of simultaneous linear equations. One also could use larger number of polynomial coefficients in PIC or Fourier terms in WIC, than the minimum number required to satisfy the zero residual vibrations and smoothness conditions, and use these excess terms to enhance the robustness.

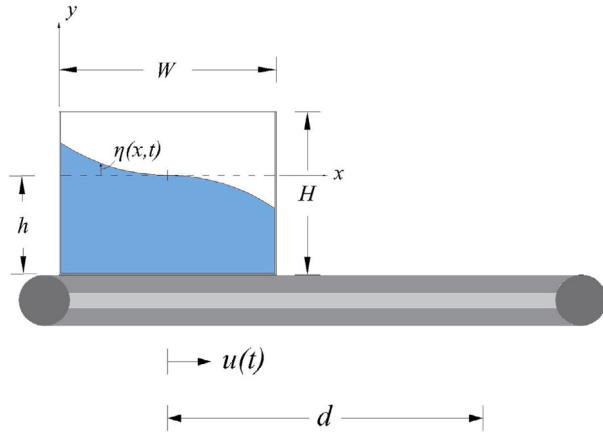


Fig. 1. A rigid-walled water-filled container.

#### 4. Illustrative examples

The performance and effectiveness of these two proposed shaped commands are demonstrated using two examples. First, a water-filled container is used to demonstrate the effectiveness of the proposed shaped commands designed based on the lower modes to eliminate residual sloshing from the higher unmodeled modes. Second, the residual vibrations of the oscillation angles in a nonlinear multiple pendulum system are eliminated numerically and experimentally using shaped commands designed from the linear resonant frequencies.

##### 4.1. Sloshing suppression of a moving water-filled container

A rigid-walled container of width  $W = 20$  cm (in the direction of wave motion) is filled with a water of depth  $h = 2$  cm (measured from the bottom of the container to the undistributed water surface,  $y = 0$ ) as shown in Fig. 1. The container is moved horizontally by means of a driven-motor with a proposed predefined acceleration command,  $\ddot{u}(t)$ . The maximum acceleration,  $a_{\max}$ , and the maximum velocity,  $v_f$ , of the driven-motor in this numerical experiment are  $1 \text{ m/s}^2$  and  $0.2 \text{ m/s}$ , respectively and the total travel distance is  $d = 0.25 \text{ m}$ .

###### 4.1.1. Governing equations

The free-surface elevation of the inside water due to the sloshing assuming irrotational flow field, nonviscous homogeneous and incompressible fluid, small free-surface displacement and velocity, and rigid and impermeable container's walls can be expressed as [17]

$$\eta(x,t) = \sum_{i=1}^N \frac{(2i-1)\pi}{W} \sinh\left(\frac{(2i-1)\pi h}{W}\right) \cos\left(\frac{(2i-1)\pi x}{W}\right) q_i(t) \quad (19)$$

where  $q_i(t)$  are time-dependent functions and are the solutions of the following differential equations,

$$\ddot{q}_i(t) + 2\zeta_i \omega_{n,i} \dot{q}_i(t) + \omega_{n,i}^2 q_i(t) = \frac{4W}{\pi^2(2i-1)^2 \cosh((2i-1)\pi h/W)} \ddot{u}(t), \quad i = 1, 2, \dots, N \quad (20)$$

where  $\omega_{n,i}$  and  $\zeta_i$  are the sloshing natural frequencies and water damping coefficient, and is equal to  $\zeta = 0.01$  [35]. The water sloshing frequencies as function of the container's width,  $W$ , and water depth,  $h$ , are given as [36]

$$\omega_{n,i} = \sqrt{\frac{(2i-1)\pi g}{W} \tanh\left(\frac{(2i-1)\pi h}{W}\right)}, \quad i = 1, 2, \dots, N \quad (21)$$

where  $g$  is the gravitational constant and  $N$  is the number of sloshing modes. The shaped PIC and WIC are generated from the natural frequencies determined from Eq. (21) for a certain number of sloshing modes. Once the acceleration input profiles,  $\ddot{u}(t)$ , are designed, the elevation of the water free-surface is determined from Eq. (19) using  $N = 9$  sloshing modes in order to demonstrate the effect of the unmodeled higher modes. The critical location where the spillage is most likely to occur is at the container's edges,  $x = 0$  or  $W$ .

The cycles in rest-to-rest maneuvers consist of acceleration, cruising, and declarations stages. It is intended to accelerate the water-filled container from a rest position to the cruising velocity,  $v_f$ , with no induced residual sloshing in the cruising stage. Therefore, the constraint here is that the motor has to reach its cruising velocity,  $U = v_f$ , at the end of the command duration. The container is then decelerated from the constant cruising velocity to the final rest position at the end of the traveled distance. Utilizing

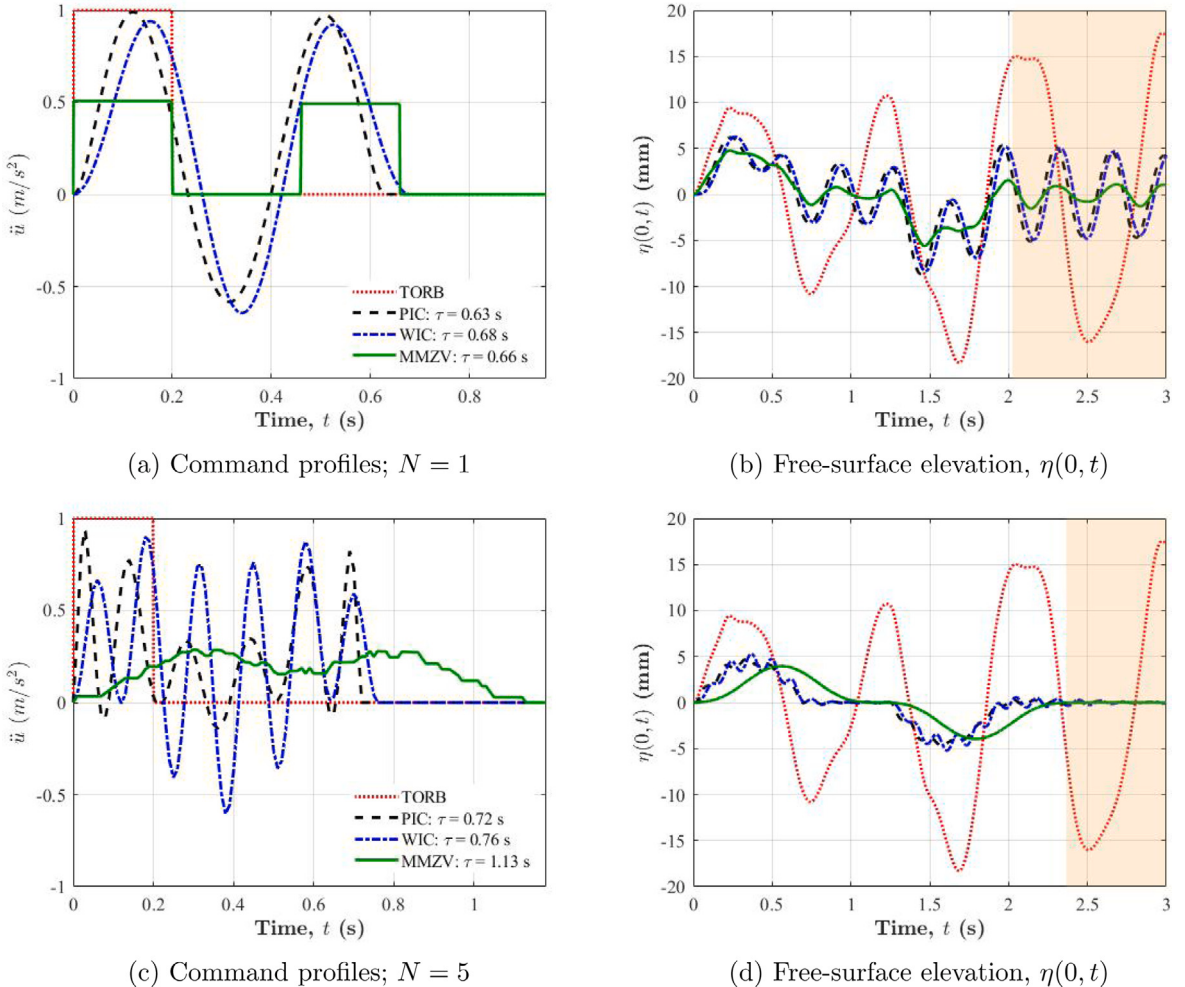
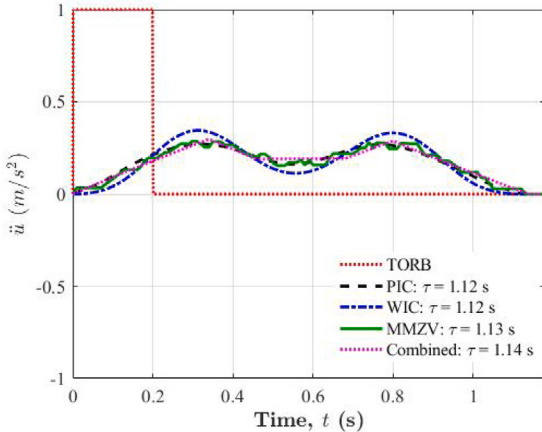


Fig. 2. Free-surface water elevations of the proposed shaped commands designed using  $N = 1$  and 5 sloshing modes and the shortest command time length.

the full capabilities of the driven-motor guarantees the achievement of an optimum command, i.e., minimum maneuver time,  $T$ . Therefore, the minimum command time length is selected such that the maximum amplitudes of the shaped commands are within the predefined maximum value of the motor acceleration, i.e.,  $a_{\max}$ . Once the shaped command is designed, the acceleration traveled distance,  $s_a$ , can be directly determined from integrating the acceleration profile. In order to bring the container to a complete stop at the target point, the shaped profile in the deceleration stage is the inverted of the acceleration profile, i.e.,  $\ddot{u}_d(t) = -\ddot{u}(t)$ . Therefore, the traveled distances in the acceleration,  $s_a$ , and deceleration,  $s_d$ , stages and their corresponding time intervals,  $\tau_a$  and  $\tau_d$ , respectively, are equal. To ensure that the container moves the total travel distance  $d$ , the cruising distance is  $s_c = d - 2s_a$ , and the corresponding time interval is  $\tau_c = s_c/v_f$ . If the command interval,  $\tau$ , is relatively long or the maneuver distance,  $d$ , is short, the shaped command may not utilize the full actuator capabilities (acceleration and/or velocity).

#### 4.1.2. Numerical simulation

Time-optimal of rigid-body (TORB) command which represents the fastest possible command profile is considered here as the reference case of the uncontrolled (unshaped) command. TORB utilizes the full input acceleration and velocity capabilities of the actuator regardless of the output response. To demonstrate the importance of considering higher frequencies when controlling multi-mode damped system, Fig. 2 illustrates the free-surface water elevation when using the shaped profiles designed based on  $N = 1$  and 5 sloshing modes and the shortest command time length; corresponding to the acceleration profile whose maximum value is not exceeding  $a_{\max}$ . The shaded areas in Fig. 2 represent the residual sloshing. The shaped command designed based on a convolved multi-mode input shaper (MMZV) is included for sake of comparison only [11]. It is clear that the convolved shaper does not utilize the input capability and its command length depends on the system parameters; natural frequency and damping ratio. The command time lengths of the convolved shaper are equal to  $\tau = 0.66$  and 1.13 s for  $N = 1$  and 5, respectively. Hence, the PIC and WIC are 56.9% (0.63 s vs. 1.13 s) and 48.8% (0.76 s vs. 1.13 s) faster than the MMZV shaper, respectively, when using  $N = 5$  sloshing



(a) Command profiles

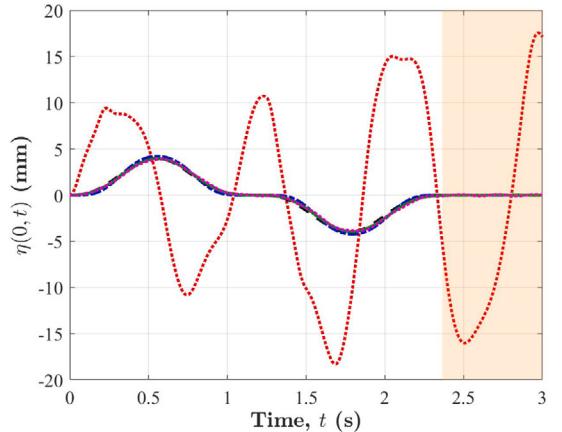
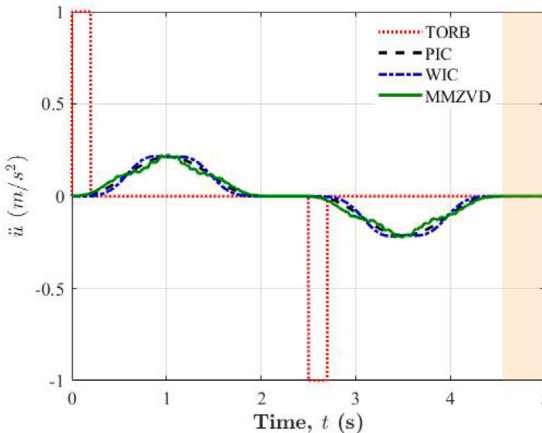
(b) Free-surface elevation,  $\eta(0, t)$ 

Fig. 3. Free-surface water elevations of the proposed shaped commands designed using  $N = 5$  sloshing modes and a command time length of  $\tau = 1.12$  s.



(a) Command profiles

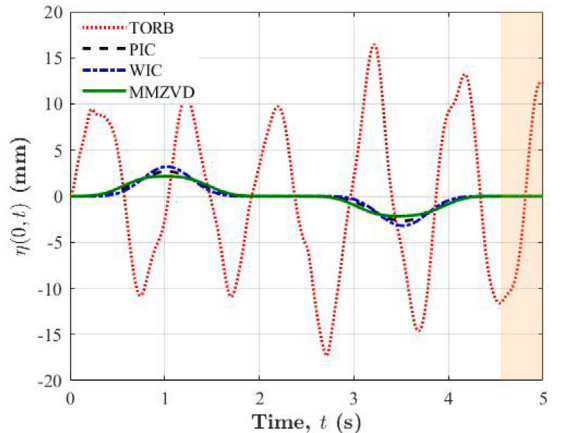
(b) Free-surface elevation,  $\eta(0, t)$ 

Fig. 4. Comparison between the free-surface water elevations of the proposed shaped commands with a command time length of  $\tau = 2.06$  s and MMZVD.

modes in the command-designing. Neglecting the effect of higher sloshing modes does not guarantee the complete elimination of the residual vibrations. Even though the command based on the primary sloshing mode is usually faster than the shaped command designed based on multiple modes, the reduction in the residual vibration from the latter is significant. Therefore, it is necessary to consider the higher modes in designing a shaped command for eliminating residual vibration of multi-mode damped systems.

Fig. 3 demonstrates a comparison between the proposed shaped commands and a smooth command designed from a combination of low-pass and multi-notch filter (zero-vibration input shaper) [17]. The command time length of this combined command depends also on the system natural frequencies and damping ratios and is equal to  $\tau = 1.14$  s. For fair comparison, the shaped commands were designed using a command time length of  $\tau = 1.12$  s, Fig. 3. Furthermore, Fig. 4 demonstrates a comparison between a multi-mode zero-vibration derivative (MMZVD) and the two proposed shaped commands using five sloshing modes. The corresponding command time length of the MMZVD is 2.06 s. To have rest-to-rest maneuver, MMZVD was convolved with bang-gang command, and hence, it consists of  $2(3^N)$  impulses, i.e., 486 steps for  $N = 5$ . To ensure that the MMZVD utilizes the maximum speed of the motor, the total traveled distance was increased to  $d = 0.5$  m. The comparisons in Figs. 3 and 4 demonstrates the capability of the proposed command in adjusting their command time length to compensate between the desired performance, command robustness, and the total move time. Unlike the smooth command in [17] that was designed assuming that the higher modes are multiples of the fundamental frequency, the shaped PIC and WIC can be designed for any values of the natural frequencies.

#### 4.1.3. Sensitivity analysis

To further assess the performance of these shaped commands, their sensitivities to the changes in water depth are investigated. Shaped commands based on a specified water depth is applied to convey a water-filled container that has different water depths.

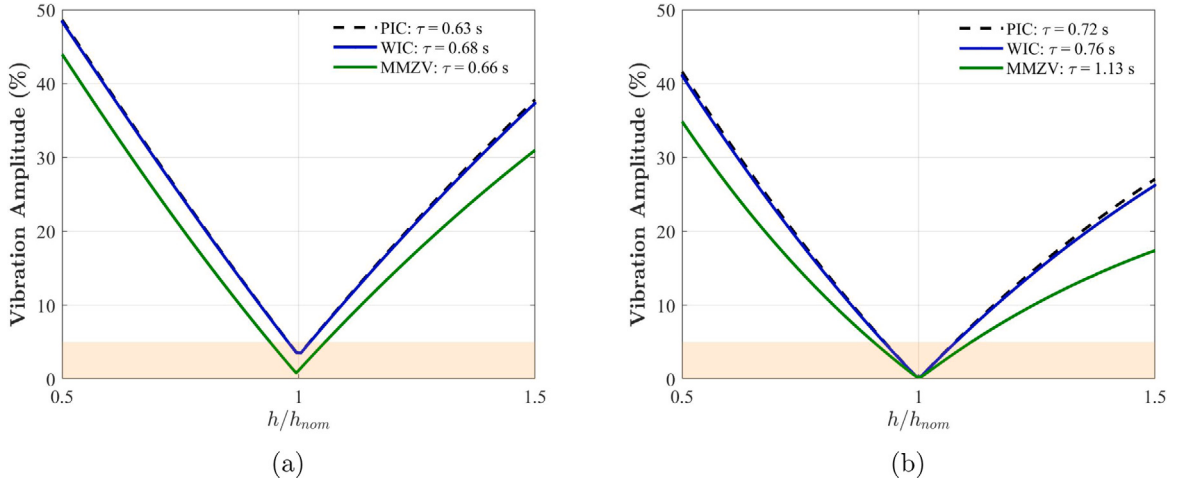


**Fig. 5.** Sensitivity curves of the shaped commands with the variation in water depths when using the shortest command time length and (a)  $N = 1$  and (b)  $N = 5$  sloshing modes.

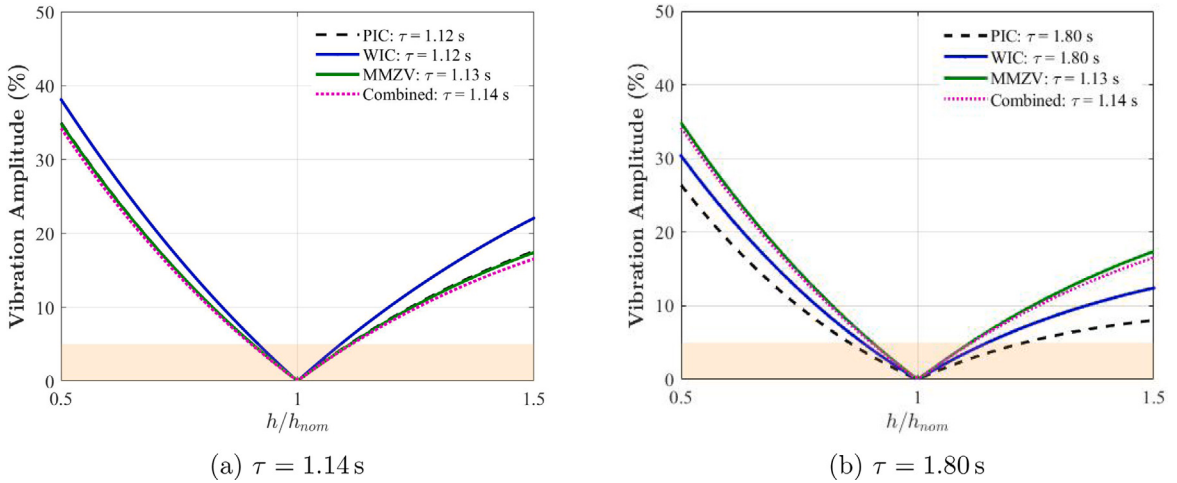


**Fig. 6.** Sensitivity curves of the shaped commands with the variation in water depths when using  $N = 5$  sloshing modes and different command lengths.

**Fig. 5** demonstrates the percentages of the residual vibration amplitudes, Eq. (17), to that induced from TORB for the three shaped commands designed based on  $N = 1$  and 5 sloshing modes and the shortest command time length. The operating depth was varied in the range of  $\pm 50\%$  from the nominal depth,  $h_{nom}$ . The shaded areas in **Figs. 5** and the subsequent figures represent the 5% tolerable residual vibration. The sensitivity curves are similar to the curves of MMZV shaper. It is clear from the figure that the shaped commands designed using the higher modes have better performance than those designed based only on the fundamental sloshing mode. Even though employing higher modes in command-designing slows down the system, it significantly reduces the transient and residual vibrations and enhances the command robustness. This demonstrates the importance of considering the higher modes when controlling a multi-mode system.

**Fig. 6** demonstrates the advantage of selectable command length in enhancing the robustness of the shaped commands where the sensitivity curves for the MMZV and smooth combined commands were included for sake of comparison. **Fig. 6(a)** shows that relaxing the proposed shaped commands ( $\tau = 1.12$  s) enhances the command robustness and makes it comparable with MMZV ( $\tau = 1.13$  s) and smooth combined ( $\tau = 1.14$  s) commands. **Fig. 6(b)** demonstrate the advantage of the selectable command length in increasing the command insensitivity. Therefore, the reduction in the transient deflection and the enhancement in the command robustness compensate the increase in the operational time.

In addition of employing the higher modes in the command-designing and relaxing the command time length to enhance the command robustness, the effect of imposing the constraints of zero-vibration and zero-derivative of the sensitivity curve and introducing two virtual frequencies adjacent to the fundamental sloshing frequency is shown in **Fig. 7**. It is clear that the variation of the residual vibration amplitude is flatten at and near the modeling depth, **Fig. 7(a)**. The robustness range is  $0.7 \leq h/h_{nom} \leq 1.4$  when

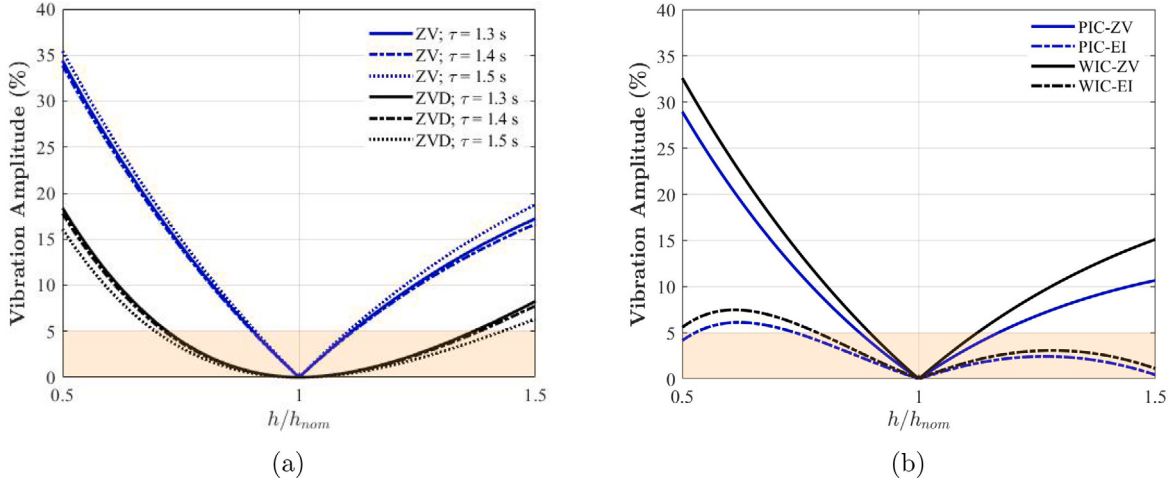


**Fig. 7.** Sensitivity curves of the shaped PIC with the variation in water depths when (a) imposing zero-vibration and zero-derivative constraints and (b) adding virtual frequencies adjacent to the fundamental sloshing frequency ( $\tau = 1.60$  s).

using the zero-derivative constraint and  $0.90 \leq h/h_{nom} \leq 1.12$  without using this constraint. To have fair comparison, both shaped commands were designed using the same command length. The enhancement of the command robustness comes with price of longer command length compared to the optimum command with only zero residual vibration. It is worth mentioning that the PIC with zero residual vibration (ZV) was designed based on five sloshing modes where PIC with zero-vibration and zero-derivative (ZVD) was designed based on three sloshing modes in addition of employing the condition of Eq. (18) at the fundamental sloshing frequency, Fig. 7(a). Similarly, the insensitivity range was enhanced when introducing two virtual frequencies (referred to as Extra-Insensitive command) corresponding to the fundamental sloshing frequencies at depths of  $0.5h_m$  and  $1.5h_m$ , Fig. 7(b). To have fair comparison regarding the number of employed designed frequencies, only the first three sloshing frequencies at the modeled depth,  $h_m$ , were employed. Again, both shaped commands have the same command length of  $\tau = 1.60$  s. It is clear that the bandwidth of the reduced sensitivity increases significantly when introducing the additional virtual frequencies compared to the original shaped commands.

#### 4.2. Multiple pendulum system

The second considered example is a multiple pendulum system with  $N$  concentrated masses,  $m_i$ , joined by rigid massless ropes of length  $l_i$  as shown in Fig. 8. The upper mass,  $m_1$ , is attached to a moving jib (slider) whose motion,  $ii(t)$ , is controlled by a variable speed motor. The multiple pendulum system is usually used to model the dynamics of the gantry crane system [37].

##### 4.2.1. Governing equations

The governing nonlinear equation of motion corresponding to the mass  $m_i$  is given as [31]

$$\sum_{j=1}^N \sum_{\substack{p=i \\ p \geq j}}^N m_p l_i l_j \left( \ddot{\theta}_j \cos(\theta_i - \theta_j) + \dot{\theta}_j^2 \sin(\theta_i - \theta_j) \right) + g l_i \sin \theta_i \sum_{p=i}^N m_p = \ddot{u} l_i \cos \theta_i \sum_{p=i}^N m_p \quad (22)$$

where  $\theta_i$  are the clockwise oscillation angle of the mass  $m_i$  from the negative  $y$ -direction, Fig. 8. The unavailability of the system natural frequencies in Eq. (22) necessitates the need of using the linear frequencies in the command-designing. Once the acceleration input profile,  $\ddot{u}(t)$ , of the horizontal jib are designed from the linear natural frequencies, the nonlinear model, Eq. (22), is used to obtain the numerically-predicted oscillation angles for each of masses  $m_i$ .

##### 4.2.2. Numerical simulation

For the current simulation experiment, the jib has a maximum acceleration of  $a_{max} = 0.9 \text{ m/s}^2$  and a maximum velocity of  $v_f = 0.3 \text{ m/s}$  with total travel distance of  $d = 0.55 \text{ m}$ . The shaped acceleration command profiles of the moving jib are designed using the two proposed shaped commands; PIC and WIC. The constraint in this model is the maximum velocity of the jib, i.e.,  $U = v_f$ , such that the shaped command accelerates the jib to its maximum velocity. The deceleration profile of the jib is the inverted of the acceleration profile in order to bring the jib to a complete stop at the end of the maneuver. The responses of the multiple pendulum system to the different shaped commands are compared to the response of the TORB command.

Quintuple pendulum model whose parameters are given in Table 1 is used to test the performance of the proposed shaped commands in eliminating the residual oscillation of the pendulum angles. A command length of  $\tau = 1.12 \text{ s}$  corresponding to the optimum profiles in terms of maneuvering speed is used to design the shaped commands as illustrated in Fig. 9(a). It is clear from the figure that the shaped commands have the same profiles. Therefore, the numerically-predicted oscillation angles of all the

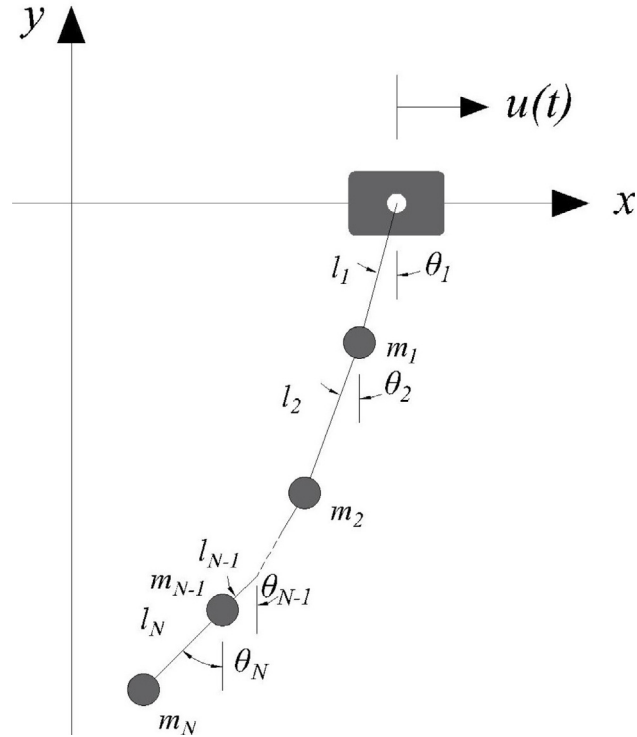


Fig. 8. Multiple pendulum system.

**Table 1**  
System parameters of quintuple pendulums.

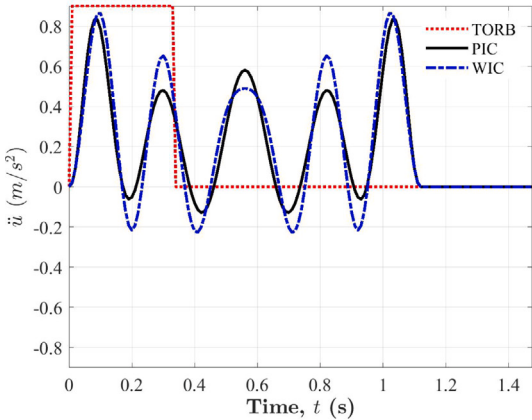
Pendulum	1	2	3	4	5
<b>Masses and cable lengths</b>					
<i>m</i> (kg)	0.21	0.11	0.21	0.11	0.11
<i>l</i> (m)	0.15	0.15	0.10	0.10	0.10
<b>Natural Frequencies, <math>\omega_{n,i}</math> (rad/s)</b>					
Numerical - Linear Model	4.71	10.3	17.4	20.9	30.6
Experimental - FFT	4.61	10.1	17.5	22.1	31.0

pendulum as shown in Figs. 9(b) through 9(f) are similar. Transient vibrations of the oscillation angles were significantly reduced compared to the TORB command. The residual vibrations in all of the oscillation pendulum angles were completely eliminated. The results demonstrate the ability of the proposed multi-mode shaped commands to reduce transient vibration and diminish residual vibrations regardless of the system degrees of freedom.

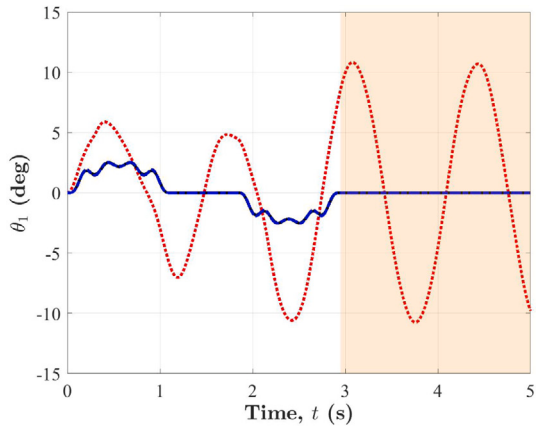
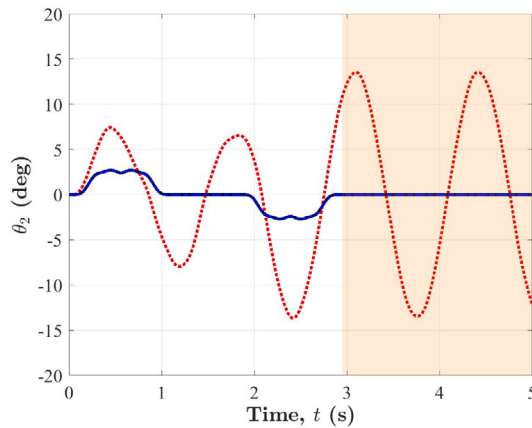
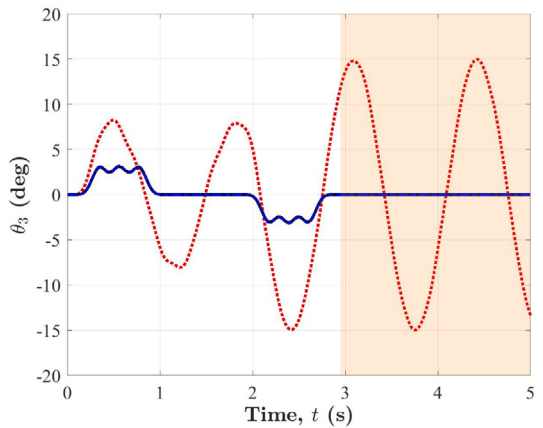
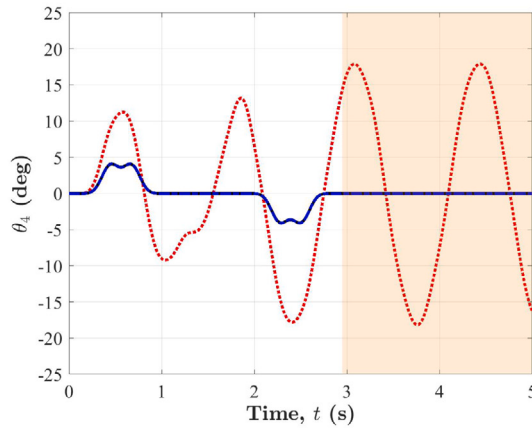
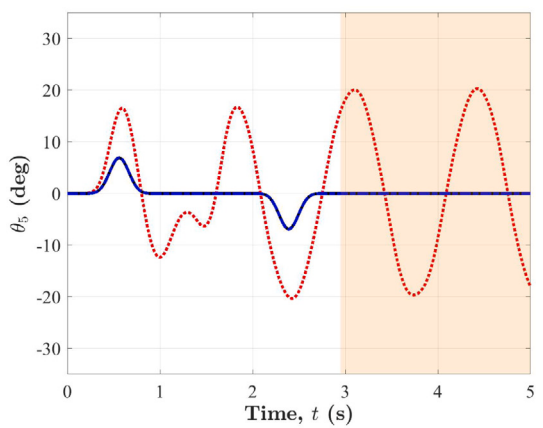
To further demonstrate the effectiveness of the proposed shaped commands, Fig. 10 compares the simulated response of MMZV command whose time length is 1.72 s with the simulated responses from PIC and WIC designed using the same command length. Even though that the MMZV command reduces and eliminates the transient and residual oscillations, respectively, the shaped PIC and WIC can be designed with a command time length that is 53.6% faster (1.12 vs 1.72 s) than the MMZV while still eliminating the residual oscillations.

#### 4.2.3. Experimental verification

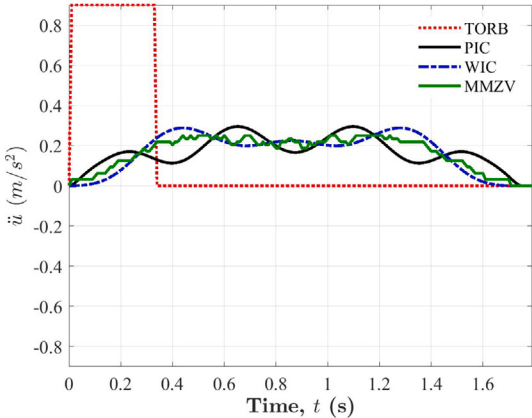
The performance of the proposed commands are validated using an actual experiment based on a scaled overhead crane model with a quintuple pendulums attached to its jib, Fig. 11. The oscillation angle corresponding to the upper pendulum is measured by a quadrature optical incremental encoder with a resolution of 1024 ppr. Knowing that the upper oscillation angle is generally a combination of all the excited modes of the other pendulums, its experimental response was used to verify the reduction of the residual oscillations from all the other remaining pendulums without the need of measuring their angles. The experimentally-determined natural frequencies using the Fast-Fourier Transform (FFT) of the oscillation angle of the upper pendulum are listed in Table 1. Even though there are small discrepancies between the experimentally-determined and numerically-evaluated natural frequencies, the latter were used instead of the former to demonstrate the efficacy of the proposed shaped commands to control the nonlinear systems using the linear resonant frequencies as far as the system is in its linear regime.



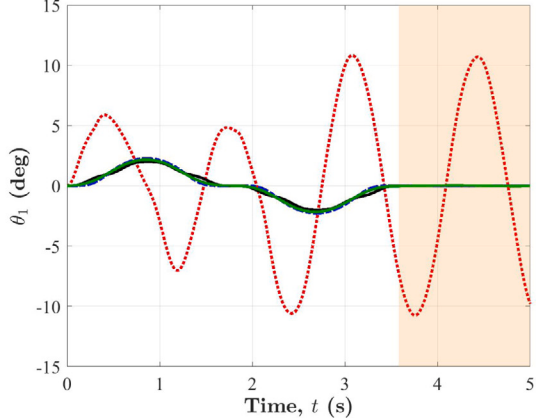
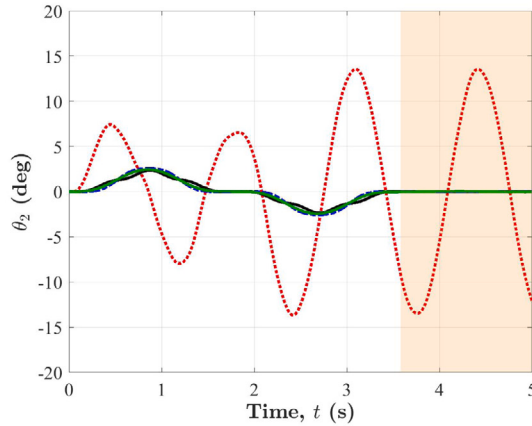
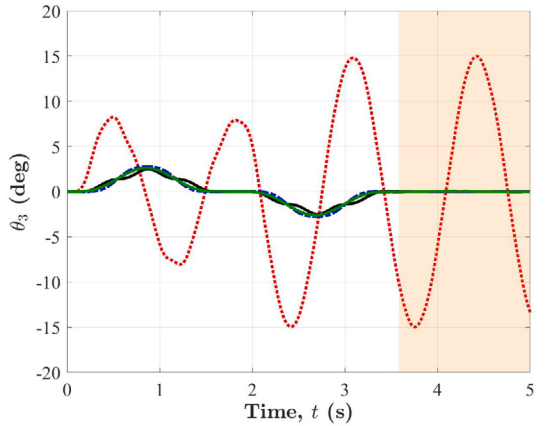
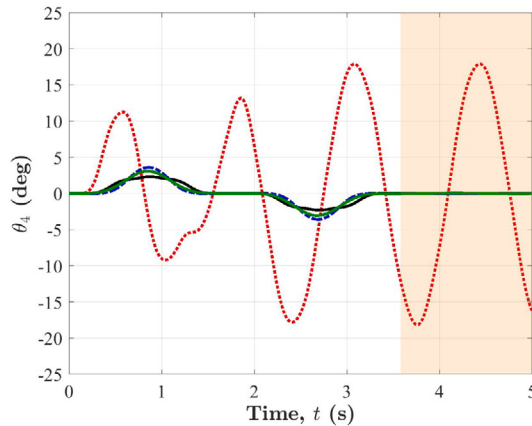
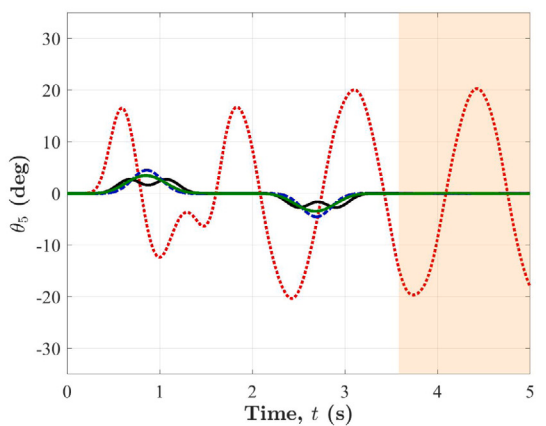
(a) Input profiles

(b) Oscillation angle  $\theta_1$ (c) Oscillation angle  $\theta_2$ (d) Oscillation angle  $\theta_3$ (e) Oscillation angle  $\theta_4$ (f) Oscillation angle  $\theta_5$ **Fig. 9.** Numerically-predicted oscillation angles of quintuple pendulum system using the proposed shaped commands with a command length of  $\tau = 1.12$  s.

**Fig. 12** shows the experimentally-measured oscillation angle of the first pendulum in a quintuple pendulum system using the proposed shaped commands with command lengths of  $\tau = 1.12$  and  $1.72$  s. The discrepancies between the experimental measurements and simulated results, **Figs. 9** and **10** compared to **Fig. 12**, are due to the fact that the mathematical model, Eq. (22), was derived assuming no friction or air resistance, massless cables, and point masses. Furthermore, other sources such



(a) Input profiles

(b) Oscillation angle  $\theta_1$ (c) Oscillation angle  $\theta_2$ (d) Oscillation angle  $\theta_3$ (e) Oscillation angle  $\theta_4$ (f) Oscillation angle  $\theta_5$ 

**Fig. 10.** Comparison of the numerically-predicted oscillation angles of quintuple pendulum system between MMZV and the proposed shaped commands when using a command time length of  $\tau = 1.72$  s.

the measurement uncertainties, the variation in the cable lengths during maneuver, input voltage, and inertial effect could also cause these discrepancies.

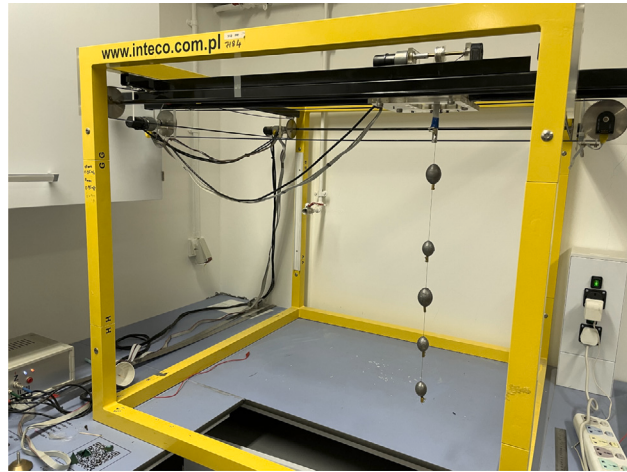


Fig. 11. Experimental setup of a quintuple pendulum system.

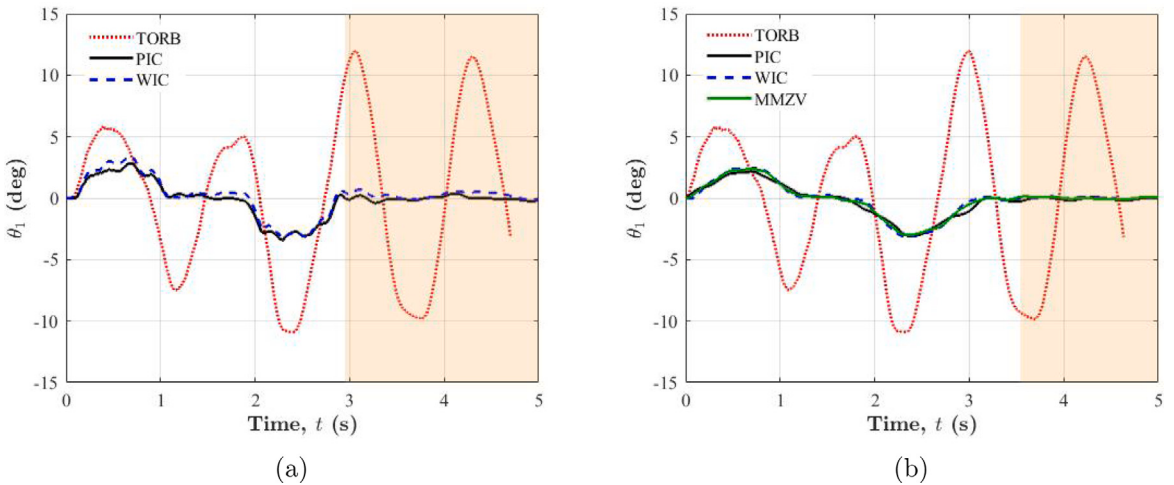


Fig. 12. Experimentally-measured oscillation angle of the first pendulum in a quintuple pendulum system using the proposed shaped commands with command lengths of (a) 1.12 s and (b) 1.72 s.

To demonstrate the effects of the higher unmodeled frequencies in the command-designing, Fig. 13(a) illustrates the measured oscillation angle of the first pendulum using PICs designed based on one, three, and five linear resonant frequencies and a command time length of  $\tau = 1.12$  s. The figure shows the importance of considering the higher modes in suppressing the residual vibrations without increasing in the transient vibration neither slowing the maneuvering operation. Fig. 13(b) demonstrates the performance of PIC and MMZV designed using one ( $\tau = 0.98$  s) and three modes ( $\tau = 1.45$  s). It is clear that the responses of PIC and MMZV designed using only the fundamental mode does not suppress the residual vibration. Even though the MMZV designed using three modes significantly suppresses the residual vibrations, the PIC has the capability to be designed using higher modes and slower command length (1.12 s vs. 1.45 s). This demonstrate the significant of the proposed command in targeting the higher modes regardless their number and with the capability of adjusting its command time length. Same conclusions can be remarked for WICs.

Even though the governing equations of the multiple pendulum system is highly nonlinear, the command shaping can be used to control the nonlinear system using the linear resonant frequencies as long as the system is varying slowly such that the linearity assumption is applied [38]. The smoothness and robustness of the proposed shaped commands overcome the variation of the natural frequency due to the nonlinearity on the vibration reduction.

#### 4.2.4. Sensitivity analysis

To complete the analysis, the sensitivity curves for the proposed commands and MMZV with the changes in the cable length that attaches the jib to the concentrated mass  $m_1$  are depicted in Fig. 14. The shaped commands have a robustness range of  $0.9 \leq l_1/l_{1,nom} \leq 1.15$  when a command length of 1.12 s is used, Fig. 14(a). The sensitivity widths increases with the increasing of the command time length, Fig. 14(b).

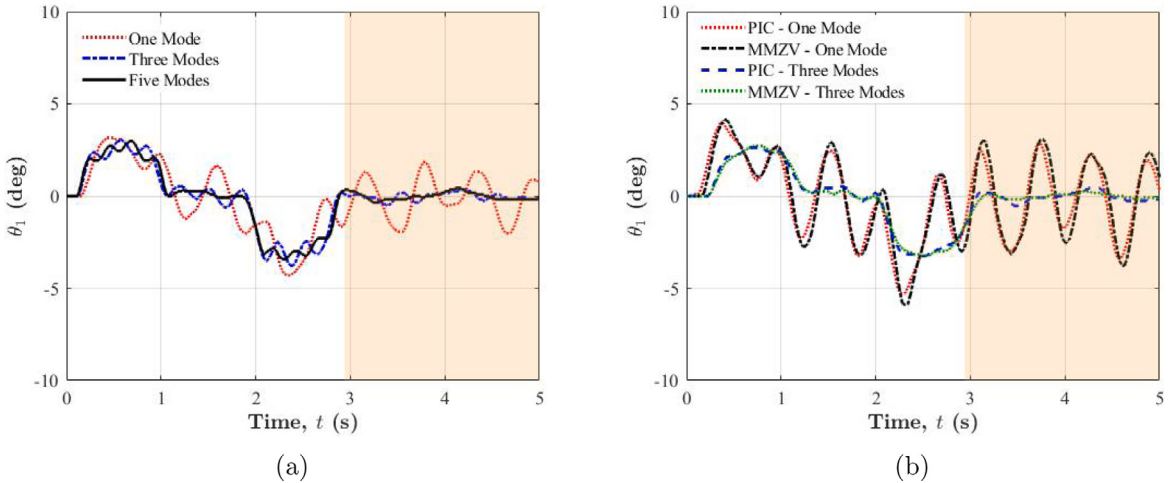


Fig. 13. Experimentally-measured oscillation angle of the first pendulum in a quintuple pendulum system; (a) using PIC and (b) comparing PIC with MMZV.

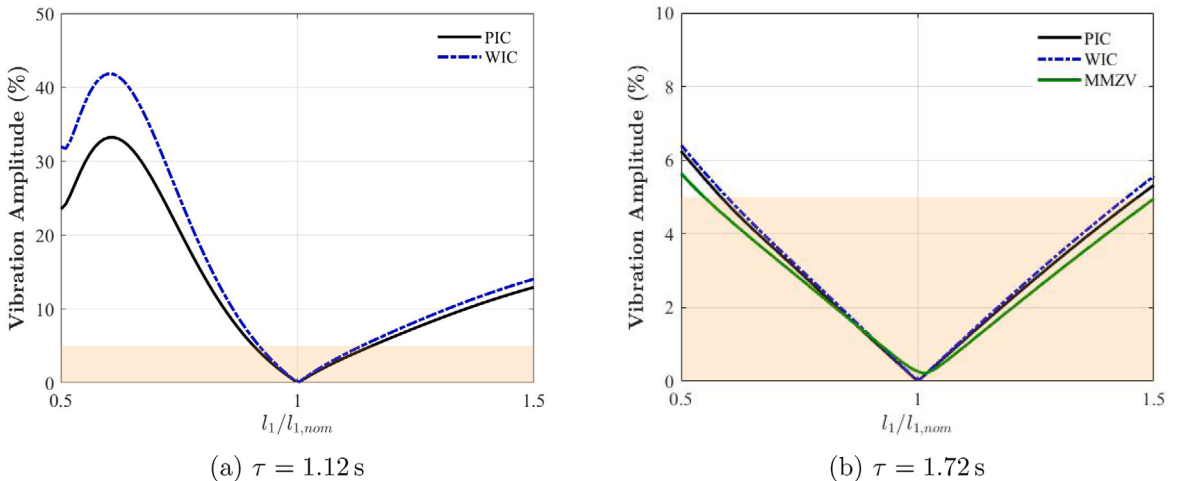


Fig. 14. Sensitivity curves of the shaped command with the changes in cable length  $l_1$  using different command lengths.

## 5. Conclusions

The proposed shaped commands generated from the general form of polynomial and waveform profiles have the ability to adjust their smoothness based on certain imposed input constraints at the beginning and the end of the command duration. The jerk-free continuous profile of these commands reduce the number of actuation actions when using single continuous command and reduce the effect of actuators delay. This ability of adjusting the command time length without any compromise in the output performance makes the shaped commands attractive in designing such optimal command that reduces the transient vibration and enhances the command robustness to compensate the increase in the operational time. Furthermore, the command time length can be selected based on the actuator's hardware sampling time and the available system power. Unlike the other multi-mode shapers that need optimization techniques to design such shaped profiles, the proposed commands were designed from solving a system of simultaneous linear equations. These commands guarantee the elimination of the residual vibrations at the end of the command duration in all modes of a multi-mode system as well as result of reduction in the induced transient vibrations. Suppressing the residual sloshing from the higher unmodeled sloshing modes in a moving liquid-filled container and eliminating the residual oscillation in a multiple pendulum system demonstrate the effectiveness of these proposed shaped commands. The commanded input can be easily integrated with other controlling scheme.

The command sensitivity demonstrates how much residual vibrations induced when errors in estimating the system frequency are present. For small changes or uncertainties in the water depth of the moving liquid-filled container and in the cable length of the multiple pendulum system, a considerable amount of residual vibration was induced. Three different approaches were proposed in enhancing the robustness of the proposed commands. The increase of command length decreases the sensitivity of the commands

to system uncertainties. Furthermore, setting the derivatives of the residual vibration amplitude with respect to the certain system natural frequencies (or damping ratios) to zero flatten the sensitivity curve at and adjacent to the modeled frequencies. Finally, introducing extra virtual frequencies around the original system frequencies increases the bandwidth of the reduced sensitivity of the system. Therefore, the variations of the operating frequencies from the modeling frequencies (because of the nonlinearities, parameter variations, model assumption, etc.) does not incur significant residual vibrations at the end of the maneuver. The time penalty of introducing a smooth robust shaped command is negligible compared to its robustness and the reduction in the transient and residual vibrations.

Unlike some multi-mode command shaping techniques which target reduction of residual vibrations, considering the higher frequencies in command-designing provides almost complete elimination of the residual vibrations. Furthermore, the proposed commands mitigate all excited vibrations regardless their numbers and values unlike combining single-mode input shaper with certain filter to tune multi-mode system frequencies where a common frequency have to be found such that all the modes are odd-multiple of that frequency. The command length of the shaped commands does not depend on the system natural frequencies and damping ratios unlike the classical input shapers.

#### Declaration of conflicting interests

The authors declare that there is no conflict of interest.

#### CRediT authorship contribution statement

**Abdullah Alshaya:** Conceptualization, Methodology, Software, Validation, Formal analysis, Investigation, Visualization, Writing – original draft. **Khaled Alhazza:** Conceptualization, Investigation, Writing – review & editing.

#### Declaration of competing interest

The authors declare that they have no known competing financial interests or personal relationships that could have appeared to influence the work reported in this paper.

#### Funding

This research received no specific grant from any funding agency in the public, commercial, or not-for-profit sectors.

#### References

- [1] N.C. Singer, W.P. Seering, Preshaping command inputs to reduce system vibration, *J. Dyn. Syst. Meas. Control* 112 (1) (1990) 76–82.
- [2] N.C. Singer, W.P. Seering, An extension of command shaping methods for controlling residual vibration using frequency sampling, in: Proceedings 1992 IEEE International Conference on Robotics and Automation, Vol.1, 1992, pp. 800–805.
- [3] C.-C. Cheng, C.-Y. Chen, Controller design for an overhead crane system with uncertainty, *Control Eng. Pract.* 4 (5) (1996) 645–653.
- [4] F. Omar, F. Karray, O. Basir, L. Yu, Autonomous overhead crane system using a fuzzy logic controller, *J. Vib. Control* 10 (9) (2004) 1255–1270, Publisher: SAGE Publications Ltd STM.
- [5] G.S. Hu, C.J. Ong, C.L. Teo, Minimum-time control of a crane with simultaneous traverse and hoisting motions, *J. Optim. Theory Appl.* 120 (2) (2004) 395–416.
- [6] W. Singhose, Command shaping for flexible systems: A review of the first 50 years, *Int. J. Precis. Eng. Manuf.* 10 (4) (2009) 153–168.
- [7] W. Singhose, R. Eloundou, J. Lawrence, Command generation for flexible systems by input shaping and command smoothing, *J. Guid. Control Dyn.* 33 (6) (2010) 1697–1707, Publisher: American Institute of Aeronautics and Astronautics.
- [8] B. Pridgen, W. Singhose, Comparison of polynomial cam profiles and input shaping for driving flexible systems, *J. Mech. Des.* 134 (12) (2012).
- [9] J. Vaughan, A. Yano, W. Singhose, Comparison of robust input shapers, *J. Sound Vib.* 315 (4) (2008) 797–815.
- [10] Y. Huang, H. Li, J. Zhou, L. Meng, Extra-insensitive shaper with distributed delays: Design and vibration suppress analysis, *J. Vib. Control* 26 (15–16) (2020) 1185–1196, Publisher: SAGE Publications Ltd STM.
- [11] J.M. Hyde, W.P. Seering, Using input command pre-shaping to suppress multiple mode vibration, in: Proceedings. 1991 IEEE International Conference on Robotics and Automation, IEEE, 1991, pp. 2604–2609 vol.3.
- [12] T. Singh, S.R. Vadali, Robust time-delay control of multimode systems, *Internat. J. Control* 62 (6) (1995) 1319–1339, Publisher: Taylor & Francis.
- [13] X. Xie, J. Huang, Z. Liang, Vibration reduction for flexible systems by command smoothing, *Mech. Syst. Signal Process.* 39 (1) (2013) 461–470.
- [14] J. Huang, Z. Liang, Q. Zang, Dynamics and swing control of double-pendulum bridge cranes with distributed-mass beams, *Mech. Syst. Signal Process.* 54–55 (2015) 357–366.
- [15] J. Ye, J. Huang, Analytical analysis and oscillation control of payload twisting dynamics in a tower crane carrying a slender payload, *Mech. Syst. Signal Process.* 158 (2021) 107763.
- [16] Z. Mohamed, M. Tokhi, Command shaping techniques for vibration control of a flexible robot manipulator, *Mechatronics* 39 (2003) 1039–1047.
- [17] Q. Zang, J. Huang, Z. Liang, Slop suppression for infinite modes in a moving liquid container, *IEEE/ASME Trans. Mechatronics* 20 (1) (2015) 217–225.
- [18] Q. Zang, J. Huang, Dynamics and control of three-dimensional Slop in a moving rectangular liquid container undergoing planar excitations, *IEEE Trans. Ind. Electron.* 62 (4) (2015-04) 2309–2318.
- [19] J. Huang, X. Zhao, Control of three-dimensional nonlinear slosh in moving rectangular containers, *J. Dyn. Syst. Meas. Control* 140 (081016) (2018) DS-17–1068.
- [20] Z. Masoud, K. Alhazza, E. Abu-Nada, M. Majeed, A hybrid command-shaper for double-pendulum overhead cranes, *J. Vib. Control* 20 (1) (2014) 24–37, Publisher: SAGE Publications Ltd STM.
- [21] M. Giacomelli, F. Padula, L. Simoni, A. Visioli, Simplified input-output inversion control of a double pendulum overhead crane for residual oscillations reduction, *Mechatronics* 56 (2018) 37–47.

- [22] H. Jaafar, Z. Mohamed, M. Shamsudin, N. Mohd Subha, L. Ramli, A. Abdullahi, Model reference command shaping for vibration control of multimode flexible systems with application to a double-pendulum overhead crane, *Mech. Syst. Signal Process.* 115 (2019) 677–695.
- [23] H.I. Jaafar, Z. Mohamed, N.A. Mohd Subha, A.R. Husain, F.S. Ismail, L. Ramli, M.O. Tokhi, M.A. Shamsudin, Efficient control of a nonlinear double-pendulum overhead crane with sensorless payload motion using an improved PSO-tuned PID controller, *J. Vib. Control* 25 (4) (2019) 907–921, Publisher: SAGE Publications Ltd STM.
- [24] Q. Wu, X. Wang, L. Hua, M. Xia, Dynamic analysis and time optimal anti-swing control of double pendulum bridge crane with distributed mass beams, *Mech. Syst. Signal Process.* 144 (2020) 106968.
- [25] Q. Wu, X. Wang, L. Hua, M. Xia, Improved time optimal anti-swing control system based on low-pass filter for double pendulum crane system with distributed mass beam, *Mech. Syst. Signal Process.* 151 (2021) 107444.
- [26] W. Singhose, L. Pao, A comparison of input shaping and time-optimal flexible-body control, *Control Eng. Pract.* 5 (4) (1997) 459–467.
- [27] M. Zhang, X. Ma, X. Rong, X. Tian, Y. Li, Adaptive tracking control for double-pendulum overhead cranes subject to tracking error limitation, parametric uncertainties and external disturbances, *Mech. Syst. Signal Process.* 76–77 (2016) 15–32.
- [28] H. Chen, Y. Fang, N. Sun, An adaptive tracking control method with swing suppression for 4-DOF tower crane systems, *Mech. Syst. Signal Process.* 123 (2019) 426–442.
- [29] A. Alshaya, K. Alghanim, Command shaping for sloshing suppression of a suspended liquid container, *J. Dyn. Syst. Meas. Control* 142 (121003) (2020).
- [30] A. Alshaya, A. Alshayji, Robust multi-steps input command for liquid sloshing control, *J. Vib. Control* (2021).
- [31] K.A. Alhazza, Z.N. Masoud, Waveform command shaping control of multimode systems, *J. Sound Vib.* 363 (2016) 126–140.
- [32] Z.N. Masoud, K.A. Alhazza, A smooth multimode waveform command shaping control with selectable command length, *J. Sound Vib.* 397 (2017) 1–16.
- [33] A. Alshaya, D. Almujarrab, A smooth polynomial shaped command for sloshing suppression of a suspended liquid container, *Trans. Inst. Meas. Control* 43 (2) (2020) 278–294.
- [34] P. Avitabile, *Modal Testing: A Practitioner's Guide*, First ed., Wiley, 2018.
- [35] H.N. Abramson, The dynamic behavior of liquids in moving containers, with applications to space vehicle technology, 1966.
- [36] E. Graham, A. Rodriguez, Characteristics of fuel motion which affect air plane dynamics, *J. Appl. Mech.* 19 (1952) 381–388.
- [37] E.M. Abdel-Rahman, A.H. Nayfeh, Z.N. Masoud, Dynamics and control of cranes: A review, *J. Vib. Control* 9 (7) (2003) 863–908, Publisher: SAGE Publications Ltd STM.
- [38] D. Blackburn, W. Singhose, J. Kitchen, V. Patrangenaru, J. Lawrence, T. Kamoi, A. Taura, Command shaping for nonlinear crane dynamics, *J. Vib. Control* 16 (4) (2010) 477–501, Publisher: SAGE Publications Ltd STM.